

# Tests of Modified Gravity with Dwarf Galaxies

Bhuvnesh Jain<sup>1</sup> and Jake VanderPlas<sup>2</sup>

## ABSTRACT

In modified gravity theories that seek to explain cosmic acceleration, dwarf galaxies in low density environments can be subject to enhanced forces. The class of scalar-tensor theories, which includes  $f(R)$  gravity, predict such a force enhancement (massive galaxies like the Milky Way can evade it through a screening mechanism that protects the interior of the galaxy from this “fifth” force). We study observable deviations from GR in the disks of late-type dwarf galaxies moving under gravity. The fifth-force acts on the dark matter and HI gas disk, but not on the stellar disk owing to the self-screening of main sequence stars. We find four distinct observable effects in such disk galaxies: 1. A displacement of the stellar disk from the HI disk. 2. Warping of the stellar disk along the direction of the external force. 3. Enhancement of the rotation curve measured from the HI gas compared to that of the stellar disk. 4. Asymmetry in the rotation curve of the stellar disk. We estimate that the spatial effects can be up to 1 kpc and the rotation velocity effects about 10 km/s in infalling dwarf galaxies. Such deviations are measurable: we expect that with a careful analysis of a sample of nearby dwarf galaxies one can improve astrophysical constraints on gravity theories by over three orders of magnitude, and even solar system constraints by one order of magnitude. Thus effective tests of gravity along the lines suggested by Hui et al. (2009) and Jain (2011) can be carried out with low-redshift galaxies, though care must be exercised in understanding possible complications from astrophysical effects.

## 1. Introduction

The true nature of the observed accelerated expansion of the universe remains a mystery, but the possible solutions to this puzzle fall into two broad categories. The first is to posit the existence of a new component of the universe with an appropriate equation of state to cause the observed acceleration. This “dark energy” may be due to an exotic particle or field, or be related to the vacuum energy of space itself. A second approach is to seek to explain this acceleration through modifications to the field equations of general relativity (GR) itself. In recent years this modified gravity (MG) approach has received attention and different approaches are being actively developed – for a review see e.g. Jain & Khoury (2010).

---

<sup>1</sup>Department of Physics & Astronomy, University of Pennsylvania, Philadelphia, PA 19104

<sup>2</sup>Astronomy Department, University of Washington, Seattle, WA 98195

A modification of GR on large (astrophysical) scales generically leads to scalar-tensor theories of gravity, where a new scalar field couples to gravity. Equivalently these theories can be described via a coupling of the scalar field to matter, which leads to enhancements of the gravitational force. Nonrelativistic matter – such as the stars, gas, and dust in galaxies – will feel this enhanced force, which in general lead to larger dynamically inferred masses. The discrepancy can be up to a factor of 1/3 in  $f(R)$  or DGP gravity. We note that photons, being relativistic, do not feel the enhanced force, so that lensing probes the true mass distribution.

This enhanced gravitational force should be detectable through fifth force experiments, tests of the equivalence principle (if the scalar coupling to matter varied with the properties of matter) or through the orbits of planets around the Sun (Will 2006). Khoury & Weltman (2004) proposed that nonlinear screening of the scalar field, called chameleon screening, can suppress the fifth force in high density environments such as the Milky Way, so that Solar System and lab tests can then be satisfied. This screening was originally suggested to hide the effects of a quintessence-like scalar that forms the dark energy and may couple to matter (generically such a coupling is expected unless forbidden by a symmetry). Hence there are reasons to expect such a screening effect to operate in either a dark energy or modified gravity scenario. Indeed, since there are only a handful of screening mechanisms (Vainshtein and symmetron screening are discussed below), small scale tests of gravity that rely on distinct signatures of screening are useful discriminators of cosmological models.

Dwarf galaxies in low-density environments may remain unscreened as the Newtonian potential  $\Phi_N$ , which determines the level of screening, is an order of magnitude smaller in magnitude than in the Milky Way. Hence dwarf galaxies can exhibit manifestations of modified forces in both their infall motions and internal dynamics. Hui et al. (2009) discuss various observational effects, in particular the fact that rotation velocities of HI gas can be enhanced. Interestingly, stars can self-screen so that the stellar disk in an unscreened dwarf galaxy may have lower rotational velocity than the HI disk. Indeed the small scale dynamics of nearby galaxies may have a bigger signal of MG than large-scale perturbations – see Jain (2011) for a discussion of observational approaches.

In this work, we discuss observable effects on disk galaxies that can arise due to their interaction with a neighbor or other sources of an external gravitational field. We focus on late-type dwarf galaxies as these are most likely to be unscreened. The basic effect is that if the stellar disk remains screened, it will lag the dark matter and HI disk in the infall towards another galaxy. This may lead to a separation of the stellar disk from the center of mass of the dark matter and from the HI disk. Distortions of the morphology and rotation curves of the stellar disk may result. Our goal is to estimate the size of these effects. A similar effect in a somewhat different context was discussed by Kesden & Kamionkowski (2006), who used tidal effects on dwarf galaxies to test the equivalence principle in the Milky Way. They were interested in tests that may reveal an additional force that acts only between dark matter particles, as were Gradwohl & Frieman (1992). We are concerned with a universal force but one that may be suppressed depending on the density of the tracer. We discuss the connections and differences of our work from these papers below.

While we do not wish to be restricted to particular models, we do work within a modified gravity scenario that relies on chameleon screening (we discuss below how the recently proposed symmetron and, in some situations, Vainshtein screening mechanisms are also testable via the effects we discuss). Further we assume that sufficiently small galaxies, of virial masses  $M \sim 10^{10} - 10^{11} M_\odot$  are unscreened. The virial radius and peak circular velocity (or velocity dispersion) scale with halo mass as  $r_{\text{vir}}, v_c \propto M^{1/3}$ . So the Newtonian potential at the virial radius scales roughly as  $|\Phi_N| \propto M/r_{\text{vir}} \propto M^{2/3} \propto v_c^2$ . The Milky Way has  $|\Phi_N| \approx 10^{-6}$  (with  $c = 1$ ), so a dwarf galaxy with a rotation speed of about 50 km/s (a factor of 4 smaller than the Milky Way) will have  $|\Phi_N| \lesssim 10^{-7}$ . We will assume that such dwarf galaxies are unscreened provided they occupy a sufficiently low density environment. Within a galaxy group or cluster, the same sized dwarf galaxy would be screened, which provides a potentially useful “control” sample. Main sequence stars happen to have  $|\Phi_N| \approx 10^{-6}$ , so stars are expected to be self-screened even inside unscreened galaxies.

We estimate analytically the displacement of the stellar disk in a dark matter halo in §2. In §3 we describe the distortions of the stellar disk and present results from simple simulations. The implications and caveats associated with these results are discussed in §4. We conclude in §5.

## 2. Two-body infall

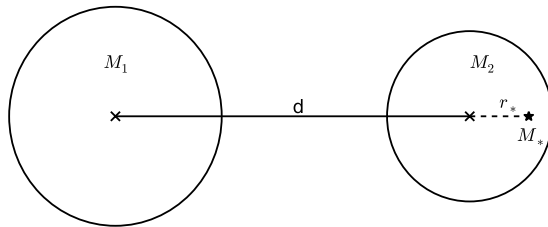


Fig. 1.— We consider the infall of a dwarf galaxy with mass  $M_2$  towards another galaxy of larger mass  $M_1$ . The stars lag the center of mass of  $M_2$  by distance  $r_*$ .

Consider a dwarf galaxy in an external gravitational field: for concreteness we will consider the force due to a neighboring galaxy, as shown in Figure 1. We are interested in the effect of the attractive “fifth” force due to a scalar field in the context of a chameleon-type screening mechanism that leaves objects with Newtonian potential  $|\Phi_N| \lesssim 10^{-7}$  unscreened. Since stars in dwarf galaxies are able to self-screen, the stellar disk can separate from the center of mass of the dark matter (DM) halo of the dwarf galaxy because the fifth force acts only on the DM.

Figure 1 shows dwarf galaxy of mass  $M_2$  falling towards another galaxy of  $M_1 > M_2$  with

$d$  being the instantaneous separation between their centers of mass. The virial radii (not labeled above) are  $r_1$  and  $r_2$ . Within  $M_2$ , the dark matter feels an enhanced force towards  $M_1$ , while the stars feel only GR. As the halos approach each other, the stars fall behind the DM with a separation that increases with time. At the moment when the galaxies are at distance  $d$ , let the stellar component of mass  $M_\star$  lag the DM by distance  $r_\star$ . Let's make the following simplifications:

1. The DM dominates  $M_2$  and the self-gravity of the stars is negligible. This is valid for most dwarf galaxies outside of the innermost  $\lesssim 1$  kpc region.
2. The force enhancement for the DM is well approximated by changing the gravitational constant to  $G > G_N$ . This is valid provided the dwarf galaxy is in an unscreened environment so that the scalar field is nearly massless.
3. We will also assume  $r_\star/d \ll 1$ . While we are interested in cases where this ratio is not negligibly small, order unity deviations are easily excluded observationally.

## 2.1. Displacement of the stellar component

Our starting point is to seek the minimum of the gravitational potential felt by the stellar disk in the reference frame defined by halo 2. The disk will rotate about this minimum, which makes it a useful estimate of the overall displacement  $r_\star$ . We will consider a star near the center of the disk here – in §3, we apply a more rigorous approach which takes into account the dynamics of a finite-sized disk.

The acceleration of  $M_2$  towards  $M_1$  is given by

$$a_2 = \frac{GM_1}{d^2} \quad (1)$$

In this accelerating reference frame, the instantaneous potential felt by a star at location  $r_\star$  is given by

$$\Phi(r_\star) = \Phi_2(r_\star) - \frac{G_N M_1}{d + r_\star} - \frac{GM_1}{d^2} r_\star \quad (2)$$

where  $\Phi_2$  is the potential due to the dark matter halo of the infalling galaxy, the second term is the effect of  $M_1$  on the star and the final term accounts for the accelerating reference frame. Minimizing this with respect to  $r_\star$ , in the limit  $r_\star/d \ll 1$ , gives

$$\frac{M_1}{d^2} \left( \frac{G - G_N}{G_N} + \frac{2r_\star}{d} \right) = \frac{M_2(< r_\star)}{r_\star^2} \quad (3)$$

Where we have used  $d\Phi_2/dr = G_N M_2(< r)/r^2$ . Care is needed here: Equation 3 describes not only the desired local minimum of the potential, but also a possible local maximum which is not a physical solution. The solution is a minimum if the second derivative of Equation 2 is positive.

Let us introduce the dimensionless parameters

$$m \equiv M_2/M_1, \quad g \equiv \Delta G/G_N = \frac{G - G_N}{G_N}, \quad \mu \equiv r_2/d, \quad \nu \equiv r_*/r_2, \quad \text{such that } r_*/d = \mu\nu \quad (4)$$

all of which are smaller than 1, but not necessarily much smaller. For given values of the other parameters, we are interested in how large  $r_*$  is (in §3 we also consider the warping effect on a finite disk and on rotation velocities): values of order a kpc would be potentially observable. We also note that typical values for the other scales are:  $r_2 \approx 20 - 50$  kpc and  $d \gtrsim 100$  kpc.

Writing Equation 3 in terms of the dimensionless parameters defined in Equation 4, we obtain

$$\mu^2 \nu^2 (g + 2\mu\nu) = m \frac{M_2(< r_*)}{M_2} \quad (5)$$

We assume the halo masses satisfy  $m < 1$ , and that the modification to gravity is order  $g \sim 1$ . If the halos have not yet collided, then we must have  $\mu \lesssim 1/2$ , depending on the relative virial radii of the halos. Finally, we expect  $\nu \ll 1$ , or this effect would likely have been observed in the past.

We can proceed by exploring a few possible forms of  $M_2(< r_*)$ . Let us first consider the case where  $M_2$  follows a power law profile:  $\rho(r) \propto 1/r^\alpha$  so that  $M_2(< r_*)/M_2 = \nu^{3-\alpha}$ . Equation 5 can then be simplified to

$$\mu^2 (g + 2\mu\nu) = m \nu^{1-\alpha} \quad (6)$$

The solution for  $\nu$  is then easy to see graphically: the LHS of Equation 6 is a straight line with a positive slope and the solution is its intersection with the RHS which is a power law that's either a positive or negative power. The negative power gives a solution for  $\nu \sim 1$  that corresponds to a local maximum of the potential, whereas we are interested in the minimum.

The problem with a steep inner profile is that with  $\alpha > 1$ , the potential diverges at  $r \rightarrow 0$ , so that the approach in Equation 3 of setting the gradient to zero will not find the true minimum. Thus we expect that for halos with steep inner profiles, the magnitude  $r_*$  of the mean separation will be negligible. The inner profile of Navarro, Frenk & White (NFW) halos is  $\alpha = 1$ , thus we expect  $r_*$  to be very small for such halos (we will see in §3 that finite sized disks in such halos nevertheless show observable effects).

Realistic dwarf galaxy halos can have shallower central profiles, the limit of which is simply a flat core. This regime can be approximated by a constant density sphere,  $\alpha = 0$ . In this case we have

$$\nu = \frac{\mu^2}{m} (g - 2\mu\nu) \approx \frac{\mu^2 g}{m} \quad (7)$$

If  $g \sim 1$ ,  $\mu \sim 1/10$ , and  $m \sim 1/8$ , we get  $\nu \sim 1/10$ . This is potentially an interesting number, as it implies  $r_* \sim 1$  kpc for typical sizes of dwarf galaxies. Real halos have core radii on the order of a few kpc, so this constant density approximation quickly breaks down. To obtain a more rigorous estimate of the expected deviation  $r_*$  we consider more realistic density profiles.

## 2.2. Realistic density profiles

The power-law profiles discussed above are overly simplistic, but they point to the existence of two regimes with very different qualitative behavior: halos with steep cores and halos with flat cores. To represent realistic dwarf galaxy halos with these properties, we will use the following two halo profiles:

**Cored Isothermal Sphere (cSIS):** A cored isothermal sphere has a flat core which, for low mass galaxies, extends up to  $\sim 1 - 4$  kpc from the center. It is a good approximation to DM halos in observed dwarf galaxies (see Swaters et al. 2011). The density profile is given by

$$\rho(r) = \frac{\rho_0}{1 + (r/r_0)^2} \quad (8)$$

Letting  $x \equiv r/r_0$ , the mass within a radius  $r$  can be expressed

$$M(< r) = 4\pi\rho_0 r_0^3 \left[ x - \tan^{-1}(x) \right] \quad (9)$$

and the potential  $\Phi$  felt by a star at radius  $r$  is

$$\Phi(r) = 4\pi G_N \rho_0 r_0^2 \left[ \frac{\log(x^2 + 1)}{2} + \frac{\tan^{-1}(x)}{x} \right] \quad (10)$$

**NFW halo:** The NFW halo is a steeper-cored profile which is well-motivated both observationally and theoretically. For a suitable choice of parameters, the NFW and cSIS profile yield rotation curves that are reasonable fits to observations over relevant radii. The NFW density profile is given by

$$\rho(r) = \frac{\rho_0}{(r/r_0)(1 + r/r_0)^2} \quad (11)$$

Again letting  $x \equiv r/r_0$ , the mass within a radius  $r$  can be expressed

$$M(< r) = 4\pi\rho_0 r_0^3 \left[ \log(x + 1) - \frac{x}{x + 1} \right] \quad (12)$$

and the potential  $\Phi$  at radius  $r$  is

$$\Phi(r) = 4\pi G_N \rho_0 r_0^2 \left[ 1 - \frac{\log(x + 1)}{x} \right] \quad (13)$$

Using these two halo profile shapes in Equation 5 gives

$$\text{cSIS : } \quad \mu^2 \nu^2 (g + 2\mu\nu) = m \frac{\nu c - \arctan(\nu c)}{c - \arctan(c)} \quad (14)$$

$$\text{NFW : } \quad \mu^2 \nu^2 (g + 2\mu\nu) = m \frac{\log(\nu c + 1) - \nu c / (\nu c + 1)}{\log(c + 1) - c / (c + 1)} \quad (15)$$

where we have defined the concentration parameter  $c \equiv r_2/r_0$ , where  $r_2$  is the virial radius of the halo.

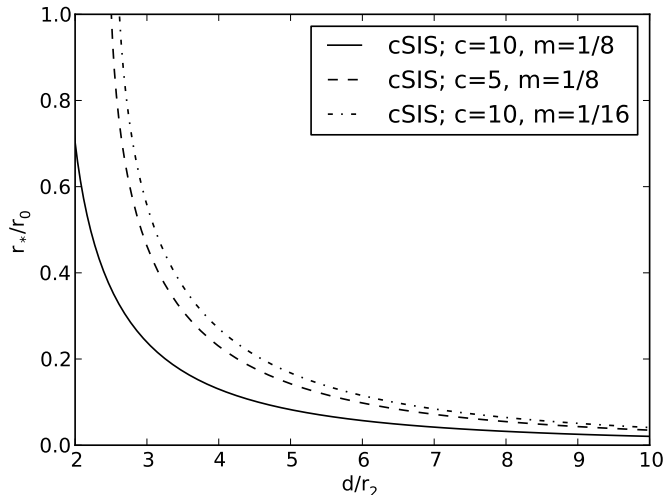


Fig. 2.— The displacement of stars  $r_*/r_0$  as a function of halo separation for the cSIS halo profile. The curves are solutions of Equation 14. With  $r_0 \gtrsim 1\text{kpc}$ , values of  $r_*/r_0 > 0.1$  are potentially observable for nearby dwarf galaxies.

We can determine the expected size of  $r_*$  for choices of the other parameters in the equation. As discussed above, the NFW profile does not give a true solution for finite  $r_*$  – we will see below that observable effects with such a cuspy profile arise only when the finite size of the disk is considered. Solutions for the cored Isothermal Sphere are shown in Figure 2: we plot the solution in terms of  $r_*/r_0$  as the core radius  $r_0$  can be inferred from observations. Solutions with  $r_*/r_0 > 0.1$  are of interest as they correspond to observable deviations in dwarf galaxies.

### 3. Dynamics within the infalling halo

In this section we study stellar orbits within the disk of the infalling halo. We will highlight several observable effects of modified gravity that arise from the effect of an external force on the structure and rotation of the finite-sized stellar disk. We first examine the orbital structure analytically and then show results from simulations of the infalling disk galaxy.

#### 3.1. Dwarf galaxy parameters

We have presented above two mass profiles for dwarf galaxy halos, the cSIS and NFW profiles. We will study three fiducial dwarf-galaxy halos based on these profiles, with parameters given in Table 1.

Table 1: Halo profile parameters for the cases studied below.

	Eqn.	$r_0$ (kpc)	$\rho_0$ ( $M_\odot/\text{kpc}^3$ )
cSIS <sub>4kpc</sub>	(8)	4	$4 \times 10^6$
cSIS <sub>2kpc</sub>	(8)	2	$1.2 \times 10^7$
NFW <sub>4kpc</sub>	(11)	4	$1 \times 10^7$

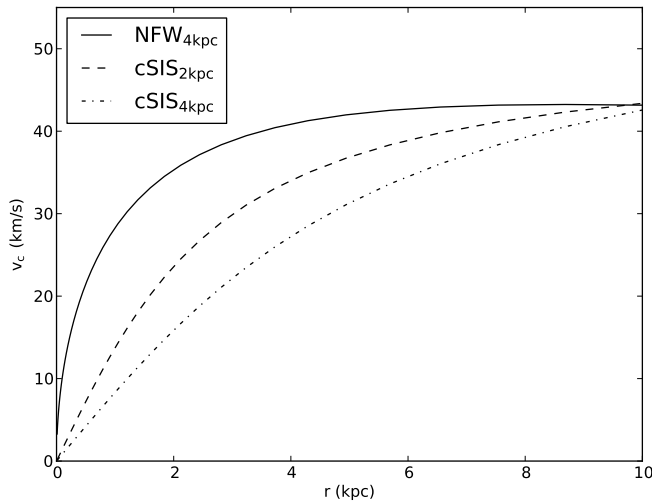


Fig. 3.— The rotation curves for our three fiducial halos, defined in §3.1: the cored Isothermal Sphere (cSIS) with core radius of 2 and 4 kpc, and the NFW profile with core radius of 4kpc. The rotation curves of NFW<sub>4kpc</sub> and cSIS<sub>2kpc</sub> are reflective of observed galaxies; cSIS<sub>4kpc</sub> is less realistic, but useful for studying the behavior of a disk within a flat core.

In order to study the behavior of a disk within a flat core, we will use the cSIS<sub>4kpc</sub> halo. The core radius of 4kpc is on the large end for low-mass galaxies (e.g. Swaters et al. 2009), but we choose it to emphasize the effects within a flat core. For a more realistic flat-core parameterization, we use the cSIS<sub>2kpc</sub> halo. For a steeper-cored case, we use the NFW<sub>4kpc</sub> halo. The core radius of 4kpc for an NFW profile is well within the typical range observed in surveys of dwarf galaxies. The rotation curves for these three fiducial cases are shown in Figure 3.

Observed late-type dwarf galaxies are rotationally supported and can be observed via their 21cm emission from the HI disk or optical data for the stellar disk. The peak rotational velocities are typically in the range  $\sim 40 - 100$  km/s, and the disk sizes range from several kpc in the optical to  $\sim 10$  kpc in HI. High resolution spatial and velocity information for galaxies at distances of  $\sim 10 - 100$  Mpc from us can provide a useful sample for the effects discussed here. Some of these galaxies are in or near groups and clusters, but there is a significant fraction that lie in the field/void environments that could be unscreened. More details on the observational sample



available currently and with forthcoming surveys will be provided elsewhere.

We will assume in what follows that the attracting galaxy has mass  $M_1 = 1.6 \times 10^{11} M_\odot$  and lies at a distance  $d = 100 \text{ kpc}$  from the infalling halo at the end of a period of infall, typically 3 Gyr. For numerical results, we set  $\Delta G/G_N = 1$ . While we assume below that the fifth force on the dwarf galaxy is due to a nearby neighbor, any unscreened or partially screened galaxy or void can provide the force.

### 3.2. Orbits in an axisymmetric potential

As discussed in §2, in the frame of the infalling halo center of mass, stars feel an acceleration which the gas and dark matter does not. We set up a coordinate system centered on the infalling halo, with halo 1 on the negative  $z$ -axis. For a star at position  $z$  (we had denoted it  $r_\star$  above), the force in the  $z$ -direction due to  $M_1$  is

$$F_z = -\frac{\partial \Phi_z}{\partial z} = \frac{\Delta G M_1}{d^2} \quad (16)$$

where, for the potential, we have approximated the final two terms of Equation 2 assuming  $z \ll d$ .

We'll assume that the stars orbit within a spherically symmetric, static background potential due to the dark matter halo. This additional force in the  $z$ -direction acts to break the spherical symmetry, resulting in an axisymmetric potential.

Consider the motion of a star in a general axisymmetric potential  $\Phi(\vec{r}) = \Phi(R, z)$ . The equation of motion is given by

$$\ddot{\vec{r}} = -\vec{\nabla} \Phi(\vec{r}) \quad (17)$$

where the dot denotes a time derivative. Transforming into cylindrical coordinates  $(R, \phi, z)$  with  $r = \sqrt{R^2 + z^2}$ , the three components of this vector equation can be equivalently expressed

$$\ddot{R} - R\dot{\phi}^2 = -\frac{\partial \Phi}{\partial R} \quad (18)$$

$$\frac{d}{dt}(R^2\dot{\phi}) = 0 \quad (19)$$

$$\ddot{z} = -\frac{\partial \Phi}{\partial z} \quad (20)$$

The second of the three equations above expresses a conserved quantity: we define the constant of motion  $L_z \equiv R^2\dot{\phi}$  and substitute this into the first equation to get

$$\ddot{R} = -\frac{\partial}{\partial R} \left[ \Phi + \frac{L_z^2}{2R^2} \right] \quad (21)$$

The terms inside the brackets on the RHS now define an effective 2D potential. Equations 20 and 21 completely define the dynamics of a test particle with angular momentum  $L_z$ : the 3D motion

has been reduced to motion in a 2D rotating plane. Examples of these two dimensional effective potentials are shown in Figure 4. As the strength of the background gravitational field increases, the minimum of the effective potential moves above the  $z$ -axis. Thus stars orbiting within the frame of halo 2 will feel a force directed away from halo 1. In the next section, we estimate the dependence of this force on the distance of the star from the halo center

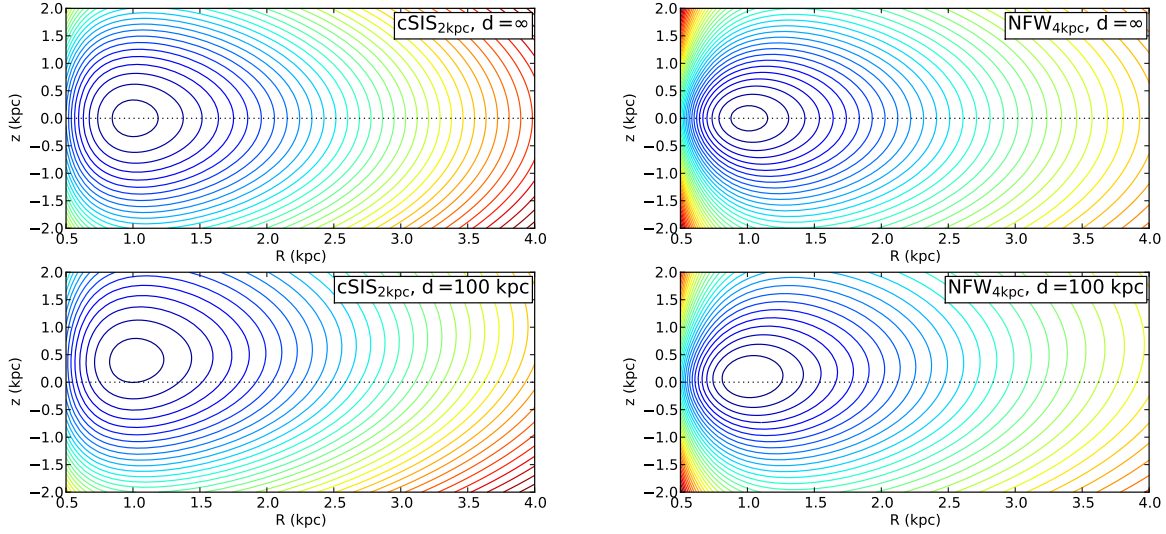


Fig. 4.— The effective potential  $\Phi_{\text{eff}}$  (Eqn. 22) in the meridional plane for the cSIS halo with  $r_0=2\text{kpc}$  (left panels) and NFW halo (right panels), for a particle with angular momentum corresponding to a circular orbit at 1 kpc. The origin in each plot corresponds to the center of the dark matter halo. As expected for the unperturbed case (upper panels), the location of the minimum is  $z = 0$ : that is, the orbits are centered on the DM halo. The lower panels show the case where the infalling halo is 100 kpc from the attracting halo. Due to the self-screening of the stars, their orbits are centered above the original plane of the disk. For the orbit shown here (1 kpc in radius), the displacement for the cSIS halo is about 0.5 kpc, much larger than for the NFW halo.

### 3.3. Orbits in the stellar disk of the infalling halo

In the dwarf galaxy encounter described above, the effective potential for a stellar orbit is

$$\Phi_{\text{eff}}(R, z; L_z) = \Phi_r(r) - F_z z + \frac{L_z^2}{2R^2} \quad (22)$$

where  $\Phi_r(r)$  is the spherically symmetric potential due to the dark matter halo (e.g. Eqns. 10 and 13),  $r = \sqrt{R^2 + z^2}$ , and  $F_z$  is the perturbing force (Eqn. 16). The minimum of  $\Phi_{\text{eff}}$  defines the position  $(R_0, z_0)$  of a circular orbit with angular momentum  $L_z$ . Orbits which are elliptical and/or

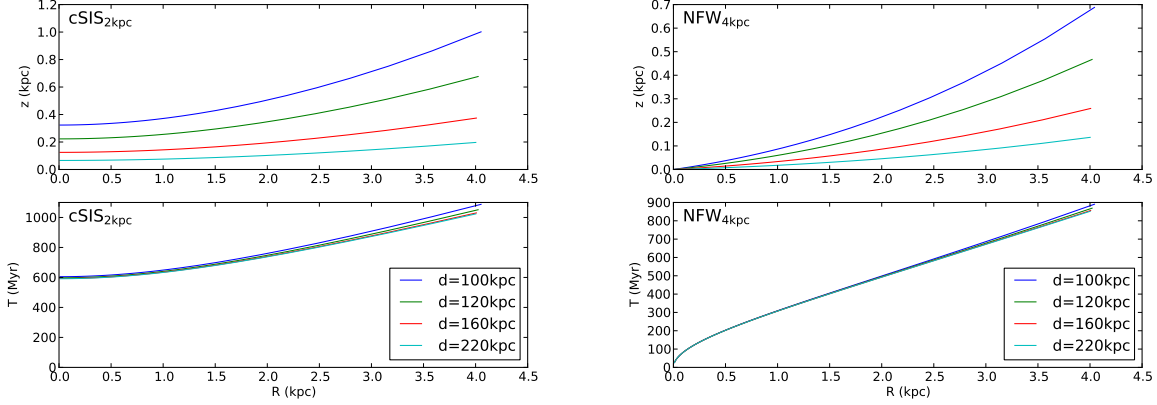


Fig. 5.— Top panels show the numerically determined relationship between  $z_0$  and  $R_0$  (Eqn. 23) for the cSIS halo with  $r_0 = 2$  kpc (left), and NFW halo (right). As the distance  $d$  decreases, the magnitude of the vertical offset increases as  $d^{-2}$ . As expected from the discussion in §3.3, the offset of the circular radius increases with  $R_0$ , and increases more steeply for the NFW case. Bottom panels show the vertical oscillation period as a function of  $R_0$  (see §3.4) calculated via Equations 25-27.

inclined will oscillate about this minimum, so it is a good first-order approximation of the mean position of stars with angular momentum  $L_z$ . Setting the partial derivatives of  $\Phi_{\text{eff}}$  with respect to  $z$  and  $R$  to zero gives

$$\begin{aligned} \left. \frac{1}{r_0} \frac{d\Phi_r}{dr} \right|_{r_0} &= \frac{L_z^2}{R_0^4} \\ \left. \frac{1}{r_0} \frac{d\Phi_r}{dr} \right|_{r_0} &= \frac{F_z}{z_0} \end{aligned} \quad (23)$$

Given an expression for the halo potential  $\Phi_r(r)$ , these equations can be solved for the position  $(R_0, z_0)$  of a star with angular momentum  $L_z$ . Let's first explore the simple case of a star in a circular orbit within the potential. A circular orbit has  $L_z^2 = (R_0 v)^2 \approx R_0 G_N M_2(< R_0)$ , where the final approximation holds for  $z_0 \ll R_0$ . Inserting this into Equations 23 gives,

$$z_0 \approx \frac{F_z R_0^3}{G_N M_2(< R_0)} \quad (24)$$

This shows that for any realistic halo, where  $M_2(< R_0) \propto R_0^\alpha$  with  $\alpha < 3$ , the mean offset should increase as a function of radius. The precise nature of this increase will depend on the exact shape of the potential.

### 3.4. Vertical oscillations

In the limit that the  $z$ -direction potential is turned on very slowly, the stellar orbits would be expected to adiabatically trace the minimum of the effective potential. Outside this limit, the perturbation of the effective potential will cause the disk to oscillate coherently in the  $z$ -direction. We can understand this oscillation by approximating the vertical shape of the potential to second order near the minimum. Then the vertical oscillation frequency can be approximated by that of a simple harmonic oscillator

$$\omega_z^2(r_0) = \frac{1}{2} \frac{\partial^2 \Phi_{\text{eff}}}{\partial z^2} \Big|_{r=r_0} \quad (25)$$

From Equation 22 we can write

$$\begin{aligned} \frac{\partial^2 \Phi_{\text{eff}}}{\partial z^2} &= \frac{1}{r} \left( 1 - \frac{z^2}{r^2} \right) \frac{d\Phi_r}{dr} + \frac{z^2}{r^2} \frac{d^2 \Phi_r}{dr^2} \\ &= \frac{G_N M_2(< r)}{r^3} \left( 1 - 3 \frac{z^2}{r^2} \right) + 4\pi G_N \rho(r) \frac{z^2}{r^2} \end{aligned} \quad (26)$$

The second line follows from Poisson’s equation and geometrical considerations. Equations 23 and 25-26 can then be used to understand the frequency of radial oscillations within a particular potential. The qualitative behavior can be seen in the limit  $z/r \ll 1$ . In this case the period of the oscillations is

$$T_z \equiv \frac{2\pi}{\omega_z} \sim \left[ \frac{R_0^3}{M(< R_0)} \right]^{1/2} \quad (27)$$

As noted above, any realistic halo will be bounded by  $M(< R_0) \sim R_0^\alpha$  with  $\alpha < 3$ . This leads generally to an oscillation period that increases with radius.

Thus for steep profiles, when the potential is turned on non-adiabatically, we expect the perturbations to cause vertical oscillations about the minimum of the effective potential with a radial phase dependence: a disk with initially near-circular orbits will display vertical waves which propagate radially outward with time.

As seen from the lower panels of Figure 5, for the outskirts of the disks in both the cSIS and NFW halos, the infall time of 3Gyr is only  $3 - 4\times$  the oscillation period: thus we expect the outer parts of the disk to display coherent vertical oscillations. In the steep inner-core of the NFW halo, the oscillation timescale is much smaller, meaning that we expect the coherence to be washed out due to orbital scatter within the disk.

### 3.5. Simulations of the stellar disk

To see all of these dynamical effects in action, we simulate the orbits of 4000 stars in a 4kpc exponential disk within the infalling halo. We allow the halo to fall from an initial distance  $d = 240\text{kpc}$  to a final distance of  $d = 100\text{kpc}$  in 3Gyr, so that the final infall speed is approximately

100km/s. The initial orbits in the disk are near circular, with a Gaussian scatter of  $\sim 1$  km/s in each direction. We integrate the orbits using the `scipy` interface to the `LSODA` routine in the `ODEPACK` library.<sup>1</sup> We make a few approximations consistent with our assumptions about dwarf galaxies in §2: first, we assume the DM in the infalling halo gives rise to a static background potential, that is, the shape of the halo does not react to the changing position of the stellar disk or the tidal effects from the distant halo. Second, we assume that the dominant force on the stellar disk is from the dark matter: we ignore self-gravitation of the disk itself.

For each halo, we try two limiting configurations: an edge-on infall and a face-on infall, as seen from the attracting galaxy. The results are shown in Figures 6-7. They lead to the following distinct observable effects (discussed further in the next section).

1. For both the edge-on and face-on cases, the mean position of the stellar disk is displaced from that of its DM halo. As expected from the discussion in §2, this displacement is on the order of  $\sim 1$  kpc for the cSIS halo, and is less pronounced for the NFW halo. Though the location of the dark matter halo is difficult to determine observationally, in this case the gas and dust in the galaxy is expected to remain unscreened, and thus track the location of the dark matter halo. This leads us to expect a separation of up to  $\sim 1$  kpc between the stellar disk and HI disk of a suitable dwarf galaxy.
2. The face-on infall cases show distinct morphological features: the galactic disks become “cup-shaped”, with the outer regions of the disk displaced further than the inner regions, as expected from the discussion in §3.3. Figure 8 shows an axially projected view of the final location of the stellar disk. The precise shape of this distortion will depend in a predictable way on two factors: the inner slope of the DM halo density profile, which can be observationally constrained from the rotation curve, and the orientation of the disk relative to the background potential, which can be deduced from dynamical surveys of nearby galaxies. The edge-on infall case shows asymmetric tidal features – the near side of the disk (relative to its neighbor) is more compact than the far side. This feature should also be kpc-scale in magnitude.
3. The asymmetry in the disk for edge-on infall is reflected in the observable rotation curves of the stellar disk (see Fig. 9). Again, this induced asymmetry in the disk rotation is expected to depend in predictable ways on the halo profile and orientation with respect to surrounding structure: in particular, the rotation curve is more extended on the far side of the disk.
4. Finally, because we generally expect the gaseous components of the galaxy to remain unscreened, the observed rotation of the HI disk will be enhanced by a factor of  $\sqrt{1 + \Delta G/G_N}$  relative to that of the stellar disk. The magnitude of this enhancement depends on the pa-

---

<sup>1</sup><http://www.scipy.org>

rameters of the MG theory, but may be as much as 20-40% as shown in Figure 9. This effect should be associated with the morphological and dynamical effects mentioned above.

## 4. Discussion

### 4.1. Summary of results

We have presented four different observable effects of gravity in MG theories on small disk galaxies: displacement of the stellar disk relative to the center of mass of the DM and gas, cup-shaped distortions in the stellar disk, asymmetries in the stellar rotation curve, and differences in rotational velocity between stellar and HI disks.

The offset and distortion of the stellar disk (#1 and #2, above), which are up to  $\sim 1\text{kpc}$ , are potentially observable in nearby dwarf galaxies, though care must be taken to rule out non-MG effects. The displacement of the stellar and HI disks is the most promising of the morphological effects (though the resolution with which the HI disks are typically imaged may restrict this to galaxies within  $\sim 100\text{Mpc}$ ). In GR, such displacements due to ram-pressure stripping of the gas are predicted in clusters (Farouki & Shapiro 1980; Vollmer 2003), but not in voids where MG becomes important. Moreover the signal has a clear correlation with the direction of the gravitational field.

The combination of the two rotation curve effects (#3 and #4 above) provides the strongest observable test, as it corresponds to discrepancies of about  $10\text{ km/s}$  between the HI and stellar rotation curve. The discrepancy has a clear signature, as shown in Figure 9. As discussed above, the distortions shown by a particular disk galaxy are sensitive to its inner halo structure. Since the HI rotation curve does tell us about the inner mass profile, one can map the observed rotation curve to the expected deviation in the stellar disk. In addition, the signal can be distinguished from contamination from other astrophysical effects by its dependence on environment and orientation: with a sufficiently large sample of late-type dwarf galaxies, one could obtain constraints that are robust to the varied dynamical histories of the observed galaxies. The signal-to-noise can be improved with a sample of galaxies that are expected to be unscreened.

The magnitude of these predicted effects will depend on various parameters of the disk galaxy and the theory: 1. The morphological effects scale as  $(1 + \Delta G/G_N)$ , which is taken to equal 2 above, while the rotation curve effects have a weaker dependence as they scale as the square root of the same factor. 2. The shape of the rotation curve determines the overall offset of the stellar disk and the warping of its outer edge. 3. The observable asymmetry in the morphology and rotation curve depends on the orientation of the galaxy disk relative to its neighbor and its inclination relative to us. 4. Predicted deviations depend on the ratio of halo masses and the separation  $d$  of the galaxy centers. However, a nearby neighbor is not essential – in general the external force on a galaxy is determined by its complete environment.

## 4.2. Comparison with previous work

We introduced the work presented above in §1 by noting the connections to astrophysical tests of the fifth force and the equivalent principle. Those tests were discussed by Gradwohl & Frieman (GF) (1992), Kesden & Kamionkowski (KK) (2006) and references therein. These authors placed limits on additional interactions between the dark matter particles that are not felt by baryons. GF considered the Milky Way (MW) infall towards Andromeda (M31), while KK examined the leading and trailing tidal arms of dwarf galaxies in the Milky Way. For related effects on large-scales, see also Keselman et al. (2010).

The motivation for our work is different: we are considering tests of modified gravity theories that introduce an additional, universal interaction for all matter – one that is suppressed in massive galaxies like the Milky Way but may act on smooth dark matter and gas in smaller galaxies in low-density environments. Hence the tests within the MW and M31 considered by previous authors would not be the most powerful tests of modified gravity.

But the physical effects in dwarf galaxies described in this paper would qualitatively apply to the MW and M31 stellar disks. The absence of the distortions of the stellar disks of the MW and M31 and the lack of asymmetry in rotation curves places some constraints on the dark matter-only fifth force (see GF for a detailed discussion). The MW is oriented edge-on towards M31, while M31 is partially face-on (e.g. Cox & Loeb 2008), so many of the observable effects we discuss could occur. However we have not attempted to quantify the constraints on the DM-only interaction from the regularity of the disks of the MW and M31.

## 4.3. Constraints on gravity theories

The three primary screening mechanisms in the literature are chameleon, symmetron and Vainshtein screening. In Appendix A we summarize their properties and note that for astrophysical tests of the kind discussed above, chameleon and symmetron theories would show observable signatures. Vainshtein screening protects the interior of the halos of all masses, so it is not likely to show any deviations in the stellar disks (but see discussion in Appendix A).

For observational tests on small scales, as discussed in Appendix A, chameleon theories may be approximately represented by the two parameters: the coupling constant  $\hat{\alpha} \approx \Delta G/G_N$  and the value of the Newtonian potential  $\Phi_N^{\text{tran}}$  that provides the transition from screened to un-screened halos. The dwarf galaxy tests discussed here can set upper limits on  $|\Phi_N^{\text{tran}}|$  for given  $\hat{\alpha}$ .

The fact that stellar disks in the literature do not consistently show any of the deviations described above can place constraints on chameleon theories (provided  $\hat{\alpha}$  is not much smaller than unity). Published measurements of late-type dwarf galaxy images in the optical and HI as well as rotation curves based on stellar and HI data appear to have the resolution to detect the signatures discussed above (e.g. Swaters et al. 2009). A sample of up to a hundred useful galaxies is available,

which allows for tests of screened vs. unscreened dwarf galaxies with  $|\Phi_N| \lesssim 10^{-7}$ . Even a quick look at the literature rules out theories with  $\hat{\alpha}$  significantly larger than unity.

The constraints that can be obtained from dwarf galaxy observations are potentially three to four orders of magnitude stronger than the best astrophysical tests in the literature (e.g. Schmidt et al 2009 and Lombriser et al 2010 constrain the equivalent parameter of  $f(R)$  theories to be larger than about  $10^{-4}$ ). This comes with several caveats: the role of astrophysical effects which impact small scales, the robustness of our predictions (which needs verification with detailed simulations), and the translation from screened dwarf galaxy halos to the parameters of the background cosmology which has a weak model dependence (see §4.4 below). Nevertheless, observations such as the ones discussed above can constrain the parameter space of  $\hat{\alpha}$  and  $\Phi_N^{\text{tran}}$ . A more detailed study of constraints available from current observations will be presented elsewhere.

Finally we note that the tests discussed here apply to a dynamical dark energy scenario as well (Khouri & Weltman 2004): they constrain a possible coupling of the dark energy to matter, and stringent constraints would point to the existence of a new symmetry that forbids the two fields from interacting. In fact chameleon theories are already constrained by solar system tests to have a Compton wavelength close to Mpc-scales (Faulkner et al. 2007, J. Khouri, private communication). This may limit the appeal of such theories, but as far as astrophysical tests go, it implies that large-scale structure tests will not be able to detect any deviations: interactions on scales larger than  $\sim 10$  Mpc will not be affected by the scalar force. However the dwarf galaxy tests discussed above could still test fifth force effects.

#### 4.4. Remaining uncertainties and further work

This study is intended to be an initial exploration into the observable effects of general scalar-tensor gravity theories on dwarf galaxies moving within an external gravitational potential. As such, a number of questions remain.

We have relied on some simplifications in treating the orbital dynamics: in particular the self-gravity of the disk, and the interaction of the stellar and HI disks have been neglected. Ignoring the self-gravity of the stellar disk can change the results if the galaxy is not dark matter dominated on scales of the observed disk. Dwarf galaxies generically do satisfy our assumption of being dark matter dominated, but a self-consistent simulation is in order. The interaction of the stellar and HI disks is a more interesting effect to consider: we estimate that the stellar disk has sufficient surface density to partially displace the HI disk, but this depends on disk radius. So while the separation of the two disks may be lower than our estimates at small radii, this can lead to morphological changes to the HI disk in unscreened galaxies – another potentially observable effect.

We have studied only a limited range of infall scenarios. Though a useful approximation, galaxy encounters are rarely head-on. In addition, the “edge-on” and “face-on” situations probe only the extremes of the possible geometries. The majority of observed galaxy encounters will lie



between these two extremes, leading to effects in both morphology and velocity profiles. We have checked that the effects we describe are evident in infall with finite impact parameters as well. Detailed simulations that capture a wider range of infall and merger geometries would be useful.

In disk galaxies there are several potential astrophysical sources of differences in the inferred dynamics of the HI and stellar disk (gas pressure on the HI disk, scattering by a bar for the stellar disk and so on). Any interpretation of observed galaxies will need to carefully account for these. One useful observation in correcting for these effects is that they are not likely to correlate with either the direction of infall or the background potential. Thus with a large enough sample of dwarf galaxies, the effects due to modified gravity could be separated from other astrophysical effects in a robust way. A sample of hundreds of late-type dwarf galaxies, split into a “control” sub-sample of galaxies that are expected to be screened and another sub-sample that are unscreened, should provide powerful tests of gravity.

We also note that the direction of the effective force on the stellar disk is determined not just by its nearest large neighbor, but by the “local” gravitational environment: this can include voids, filaments and any large but unscreened object (Zhao et al. 2011). A relatively detailed study of the mass distribution in the local universe, coupled with simulations of nonlinear screening, is needed to determine the criterion for the force on any particular galaxy. On the other hand the sample of field dwarf galaxies is much larger if one is not restricted to having a neighboring galaxy with the right properties.

The level of screening of a galaxy can be a subtle and model-dependent question. In particular, inferences from spherically symmetric models can be misleading in certain environments. A careful mapping of simulations to the local universe can help build samples of unscreened dwarf galaxies. Indeed, as noted in Appendix A, it is possible that theories that deploy Vainshtein screening can also be tested if galaxies lie in strong enough tidal fields that the expectation of screening based on a spherical model is violated. Another possibility is to be theory-agnostic and simply use a set of observational criteria that characterize the environment of the test galaxy. Observed morphological and dynamical deviations can be correlated with the environment to search for signatures of modified gravity.

In addition to tests with late-type dwarf galaxies considered here, other tests of gravity are possible with low- $z$  galaxies. Dwarf ellipticals/spheroidals may exhibit asymmetries with a similar physical origin. They are known to have very regular structure and dynamics, which can set constraints on gravity theories. The infall of galaxies onto massive systems like groups and clusters is a potential test, especially of theories that rely on Vainshtein screening - see Hui et al. (2009), Schmidt (2010), and Jain (2011) for discussions. Observable properties of stars may also be altered by the enhanced forces in MG theories (Chang & Hui 2011; Davis et al. 2011). Additionally, if stars forming in dense clouds become partially screened, it may alter the observable properties of the resulting stellar population (M. Kesden, private communication).

## 5. Conclusion

We have presented a first study of the potential observable effects of modified gravity on the morphology and dynamics of dwarf galaxies in the nearby universe. We consider the class of scalar-tensor theories that rely on chameleon or symmetron screening to recover GR in the Milky Way – these include all  $f(R)$  models. We estimate the magnitude of four potentially observable effects:

- The spatial separation of the stellar disk from the dark matter and gas
- Distinct morphological and dynamical effects in the stellar disk
- An asymmetry in the rotation velocity curve of the stellar disks along the direction of infall.
- Differences in the rotational velocities of the stellar and gaseous disks.

Through both analytical arguments and simple orbital simulations, we show that these effects are potentially observable in nearby dwarf galaxies ( $z < 0.1$ ). In particular, we estimate the magnitude of the spatial separation and morphological distortions to be up to  $\sim 1\text{kpc}$ , and the effect on rotational velocities to be  $\sim 10\text{ km/s}$ . Though accounting for other potential astrophysical sources of these effects in an isolated case is nontrivial, one can exploit the dependence on environment and orientation in order to obtain constraints on MG with a sample of galaxies.

Dwarf galaxies have Newtonian potentials in the range  $\Phi_N \sim 10^{-8} - 10^{-7}$ . Coupled with the large force enhancements that are generically expected in MG theories on small scales, dwarf galaxies have the potential to constrain certain regions of parameter space more stringently than cosmological-scale measurements and even solar system tests.

*Acknowledgements:* We are grateful to Lam Hui, Mike Kesden, Justin Khoury and especially Mike Jarvis for several helpful suggestions. We benefited from stimulating discussions with Gary Bernstein, Mariangela Bernardi, Anna Cabre, Joseph Clampitt, Andy Connolly, Neal Dalal, Julianne Dalcanton, Kurt Hinterbichler, Kazuya Koyama, Fabian Schmidt, Masahiro Takada, Mark Trodden, Vinu Vikraman, Matt Walker and Peter Yoachim. This work is supported in part by NSF grant AST-0908027 and DOE grant DE-FG02-95ER40893.

## REFERENCES

- Chang, P., & Hui, L. 2011, ApJ, 732, 25
- Cox, T. J., & Loeb, A. 2008, MNRAS, 386, 461
- Davis, A.-C., Lim, E. A., Sakstein, J., & Shaw, D. 2011, arXiv:1102.5278
- Farouki, R., & Shapiro, S. L. 1980, ApJ, 241, 928

- Faulkner, T., Tegmark, M., Bunn, E. F., & Mao, Y. 2007, *Phys. Rev. D*, 76, 063505
- Gradwohl, B.-A., & Frieman, J. A. 1992, *ApJ*, 398, 407
- Hinterbichler, K., & Khoury, J. 2010, *Physical Review Letters*, 104, 231301
- Hu, W., & Sawicki, I. 2007, *Phys. Rev. D*, 76, 104043
- Hui, L., Nicolis, A., & Stubbs, C. W. 2009, *Phys. Rev. D*, 80, 104002
- Jain, B. 2011, *arXiv:1104.0415*
- Jain, B., & Khoury, J. 2010, *Annals of Physics*, 325, 1479
- Kesden, M., & Kamionkowski, M. 2006, *Phys. Rev. D*, 74, 083007
- Keselman, J. A., Nusser, A., & Peebles, P. J. E. 2010, *Phys. Rev. D*, 81, 063521
- Khoury, J., & Weltman, A. 2004, *Physical Review Letters*, 93, 171104
- Lombriser, L., Slosar, A., Seljak, U., & Hu, W. 2010, *arXiv:1003.3009*
- Schmidt, F. 2010, *Phys. Rev. D*, 81, 103002
- Schmidt, F., Vikhlinin, A., & Hu, W. 2009, *Phys. Rev. D*, 80, 083505
- Swaters, R. A., Sancisi, R., van Albada, T. S., & van der Hulst, J. M. 2009, *A&A*, 493, 871
- . 2011, *ApJ*, 729, 118
- Vainshtein, A. 1972, *Physics Letters B*, 39, 393
- Vollmer, B. 2003, *A&A*, 398, 525
- Will, C. M. 2006, *Living Reviews in Relativity*, 9, 3
- Zhao, G.-B., Li, B., & Koyama, K. 2011, *arXiv:1105.0922*

## A. Screening Mechanisms

The field equations of GR can be derived from the action

$$S_{\text{GR}} = \frac{1}{16\pi G_{\text{N}}} \int d^4x \sqrt{-g} R + S_{\text{matter}}[g_{\mu\nu}], \quad (\text{A1})$$

where  $g$  is the determinant of the metric tensor  $g_{\mu\nu}$ , and  $R$  is the Ricci scalar. The first term is the Einstein-Hilbert action, while  $S_{\text{matter}}$  contains all matter fields, with minimal couplings to  $g_{\mu\nu}$ .

Modified gravity theories designed to explain cosmic acceleration generically reduce to scalar-tensor theories in certain limits. The addition of a scalar field to the gravity theory leads to an additional attractive force. To produce interesting effects cosmologically while satisfying the tight local constraints on deviations from GR, these scalar fields must be screened in the solar system. There are three known mechanisms for screening a scalar field – the Vainshtein, chameleon and symmetron mechanisms – all of which exploit the fact that the matter density at a typical location in the solar system is many orders of magnitude larger than the mean cosmic density. The nonlinear equations obeyed by the scalar field are such that a large ambient density results in its decoupling from matter, thus shielding dense environments from the scalar. In short, the three mechanisms rely on giving the scalar field a large mass (chameleon), a large inertia (Vainshtein), or by weakening its coupling to matter (symmetron) (see Hui et al. 2009; Jain & Khoury 2010, for details on some of the simplified description here).

By adding a suitable self-interaction potential  $V(\varphi)$  to the action, the chameleon scalar field acquires mass which is large in regions of high density, thereby suppressing any long-range interactions. In addition to  $V(\varphi)$  chameleon theories also have a coupling  $A(\varphi)$  to matter fields - in fact a coupling arises when any scalar-tensor theory is expressed in the Einstein frame:

$$S_{\text{cham}} = \int d^4x \sqrt{-g} \left( \frac{R}{16\pi G} - \frac{1}{2}(\partial\varphi)^2 - V(\varphi) \right) + S_{\text{matter}}[g_{\mu\nu} A^2(\varphi)]. \quad (\text{A2})$$

In the Einstein frame, the scalar is not directly coupled to  $R$ , but due to the coupling of the metric to  $A(\varphi)$  the motion of bodies in free fall is no longer along geodesics.

In the Newtonian regime, using the energy density  $\rho$  conserved in the Einstein frame,  $\varphi$  obeys the equation:

$$\nabla^2 \varphi = V_{,\varphi} + A_{,\varphi} \rho \quad (\text{A3})$$

Thus, because of its coupling to matter fields, the scalar field is affected by the ambient matter density. Its profile is governed by an effective potential

$$V_{\text{eff}}(\varphi) = V(\varphi) + A(\varphi)\rho. \quad (\text{A4})$$

For suitably chosen  $V(\varphi)$  and  $A(\varphi)$ , this effective potential can develop a minimum at some finite field value  $\varphi_{\text{min}}$  in the presence of background matter density, where the mass of the chameleon field  $m_{\text{eff}}^2 = V_{\text{eff},\varphi\varphi}(\varphi_{\text{min}})$  is sufficiently large to evade local constraints.

The condition for screening in chameleon theories is  $\epsilon_{\text{chameleon}} < 1$  where the screening parameter is

$$\epsilon_{\text{chameleon}} \simeq \left| \frac{\varphi_b/2\alpha}{\Phi_N} \right| \quad (\text{A5})$$

where  $\Phi_N$  is the Newtonian potential,  $\varphi_b$  is the field value at cosmic mean density, and  $\alpha$  is the coupling constant in  $A(\varphi)$  (to be explicit, a general form of  $A(\varphi)$  can be Taylor expanded as  $A(\varphi) \simeq 1 + 2\alpha\varphi$ ). For all  $f(R)$  models  $\alpha = 1/\sqrt{6}$ , and the numerator  $\varphi_b/2\alpha \approx f_{R0}$  where  $f_{R0}$  is a parameter commonly used in the literature to constrain the model (Hu & Sawicki 2007). The strongest constraints from large-scale structure come from cluster abundances and set an upper limit of  $f_{R0} \approx 10^{-4}$  (Schmidt et al. 2009; Lombriser et al. 2010).

We can write the force enhancement in chameleon theories in terms of an additional potential due to the scalar field  $\Phi_{\text{scalar}}$  as

$$\Phi_{\text{total}} = \Phi_N + \Phi_{\text{scalar}} \approx -\frac{G_N M}{r} [1 + \hat{\alpha} E(-r/\lambda_c)] \quad (\text{A6})$$

where the Compton wavelength  $\lambda_c \equiv 1/m_{\text{eff}}$ , where  $m_{\text{eff}}$  is the effective mass of the scalar field. The function  $E$  can be approximated as a constant  $\delta$  times the exponential Yukawa suppression:  $E(x) \equiv \delta e^x$ . For distances much larger than  $\lambda_c$ , the fifth force due to the scalar contribution is exponentially suppressed. The key feature of chameleon screening is that  $\lambda_c$  is not constant but depends on the local mass distribution, in particular it is very small (less than a  $mm$ ) inside objects with large Newtonian potentials ( $|\Phi_N| \gtrsim 10^{-6}$ ), causing the scalar force to be strongly damped: such objects are screened. The exterior of such objects in a cosmological background is described by  $\delta \ll 1$  since only a thin shell near the surface acquires the scalar charge. On the other hand objects that are unscreened have  $\delta = 1$  and  $\lambda_c$  large (equal to the cosmological background value) both inside and outside. Thus dynamics within and exterior to unscreened objects is well approximated through an enhanced gravitational constant:  $G_N \rightarrow G_N(1+\hat{\alpha})$ . Note that this simplified description does not capture the behavior within the thin-shell, which may be relevant for some screened halos.

For the purposes of this study, we can describe the observational features of chameleon theories through two parameters: 1. The coupling constant  $\hat{\alpha} = \Delta G/G_N$  for unscreened objects; it is generally expected to be of order unity and is  $\hat{\alpha} = 2\alpha^2 = 1/3$  for  $f(R)$  models (Hui et al. 2009, note that it is generically expected to be larger as the value  $1/3$  is not protected from quantum corrections). 2. The value of the Newtonian potential  $\Phi_N^{\text{tran}}$  that provides the transition from screened to un-screened halos. For  $|\Phi_N| \ll |\Phi_N^{\text{tran}}|$ ,  $\delta \rightarrow 1$ , so that forces are enhanced by the factor  $(1 + \hat{\alpha})$ . For screened objects on the other hand,  $|\Phi_N| \gg |\Phi_N^{\text{tran}}|$ ,  $\delta \ll 1$  and Newtonian gravity is recovered. An upper limit on  $\Phi_N^{\text{tran}}$  maps onto the theory parameter  $\varphi_b$  for given  $\alpha$ . This is the parameter  $f_{R0}$  in  $f(R)$  theories. Thus constraints from unscreened galaxies and from cosmological scales are straightforwardly related within a screening scenario.

**Symmetron screening:** The second mechanism for hiding a scalar is achieved with symmetron fields, proposed recently by Hinterbichler & Khoury (2010). The symmetron Lagrangian is qualitatively similar to that of chameleon models, but the mechanism is different. The screening

in this case relies on a scalar field acquiring a vacuum expectation value (VEV) that is small in high-density regions and large in low-density regions. An essential ingredient is that the coupling to matter is proportional to this VEV, so that the scalar couples with gravitational strength in low-density environments, but is decoupled and screened in regions of high density. This is achieved through a symmetry-breaking potential, hence the name symmetron.

The parameter that determines whether a solution is screened or not is

$$\epsilon_{\text{sym}} \equiv \frac{M^2}{\rho R^2} = \frac{M_{\text{sym}}^2/6M_{\text{Pl}}^2}{|\Phi_N|}. \quad (\text{A7})$$

where  $M_{\text{sym}}$  is a parameter of the theory. For objects with  $\epsilon_{\text{sym}} \ll 1$  the resulting symmetron-mediated force on a test particle is suppressed by  $\epsilon_{\text{sym}}$  compared to the gravitational force. On the other hand for objects with  $\epsilon_{\text{sym}} \gg 1$ , the symmetron gives an  $\mathcal{O}(1)$  correction to the gravitational force. This behavior is very similar to chameleon screening. The quantitative difference is that symmetron screening for partially screened objects penetrates deeper into the halo (Clampitt et al, in preparation). The bottom line for astrophysical tests of gravity is that chameleon and symmetron signatures occur in similar physical situations.

**Vainshtein Screening:** The third mechanism relies on the scalar field having derivative interactions that become large in regions of high density or in the vicinity of massive objects (Vainshtein 1972; Hinterbichler & Khoury 2010). Perturbations of the scalar in such regions acquire a large kinetic term and therefore decouple from matter. Thus the scalar screens itself and becomes invisible to experiments. This Vainshtein effect is the screening mechanism that operates successfully for brane-world modifications of gravity such as the DGP model and galileon scalar field theories.

For a spherical object, Vainshtein screening is effective inside the radius

$$r_{\text{Vain}} = (r_c^2 r_{\text{Sch}})^{1/3}, \quad (\text{A8})$$

with  $r_{\text{Sch}}$  denoting the Schwarzschild radius of the source. At short distances,  $r \ll r_{\text{Vain}}$ , the extra force is suppressed compared to gravity by the factor  $(r/r_{\text{Vain}})^{3/2} \ll 1$ . The ratio of the  $r_{\text{Vain}}$  to the virial radius is larger than 1 and is constant with mass, since both radii scale as  $M^{1/3}$ .

$$r_{\text{Vain}} \gtrsim r_{\text{virial}}, \quad \text{independent of mass.} \quad (\text{A9})$$

Thus the tests discussed may not be not useful for Vainshtein theories as they rely on the dynamics of disks well inside halos. We note however that the expectations of screening for spherical objects may be violated in the presence of tidal fields, which can leave galaxies along filaments of large-scale structure unscreened (R. Scoccimarro, private communication). At large distances,  $r \gg r_{\text{Vain}}$ , the enhancement to Newtonian gravity is exactly as for an unscreened object in  $f(R)$  theories: a factor of  $1/3$ . Indeed for galaxies or clusters larger than the Milky Way, the infall of other galaxies at distances larger than the virial radius will have stronger signatures from Vainshtein theories since the extra force is not suppressed by the thin shell factor for massive hosts.

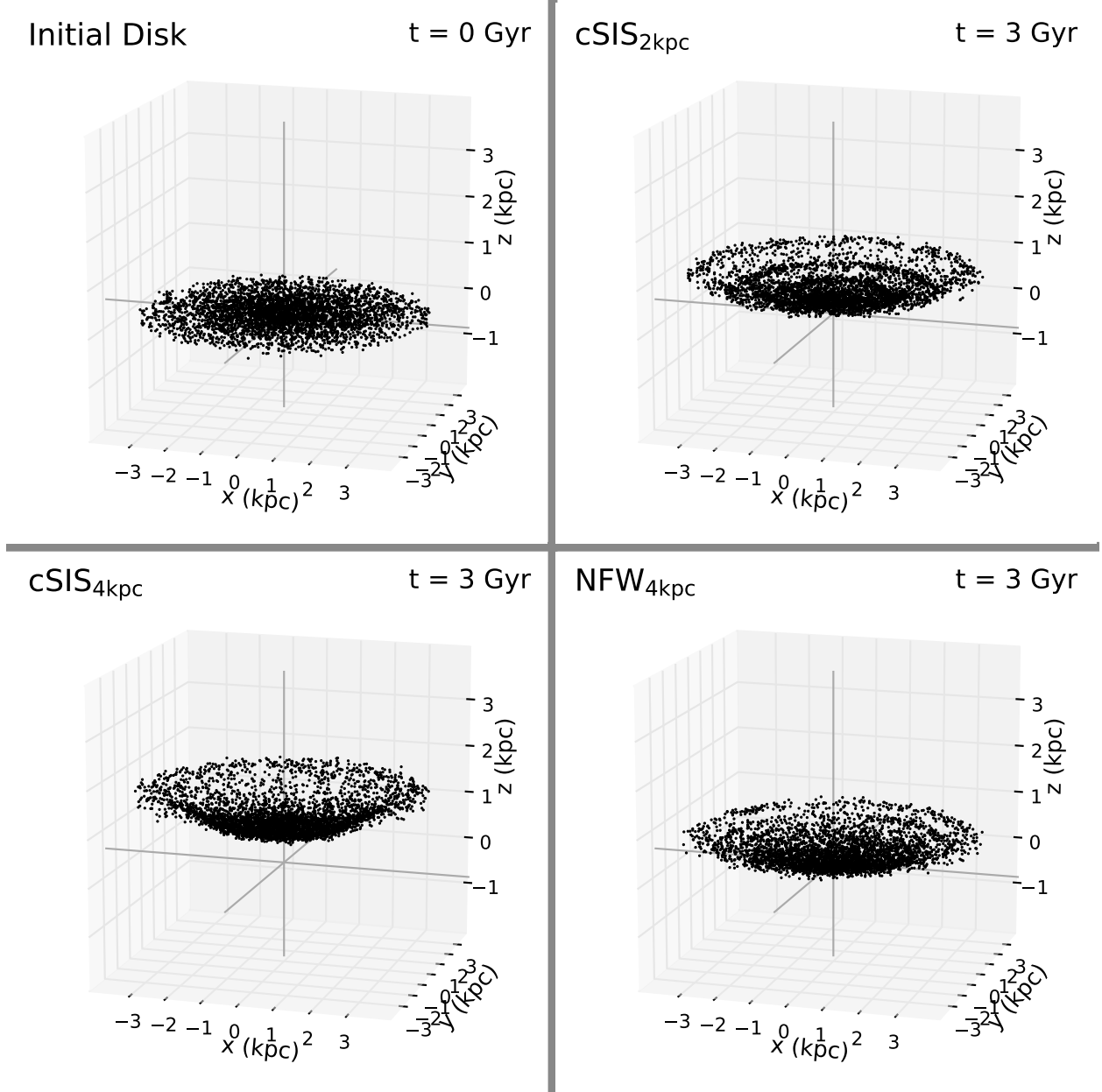


Fig. 6.— The change in the morphology of stellar disks in infalling dwarf galaxies is shown for a face-on orientation with respect to the neighboring galaxy. The initial disk is shown in the upper-left panel. The final disks for the  $\text{cSIS}_{4\text{kpc}}$ ,  $\text{cSIS}_{2\text{kpc}}$ , and  $\text{NFW}_{4\text{kpc}}$  halos are shown in the remaining panels for infall starting from a distance of 240kpc and ending 3Gyr later at a distance of 100kpc from the larger neighbor galaxy. The neighbor lies on the negative  $z$ -axis. Each dot shows the position of a star taken to be initially on a near-circular orbit. The radially averaged profiles for the face-on case are shown in Figure 8, and the rotation curves for the edge-on case are shown in Figure 9.

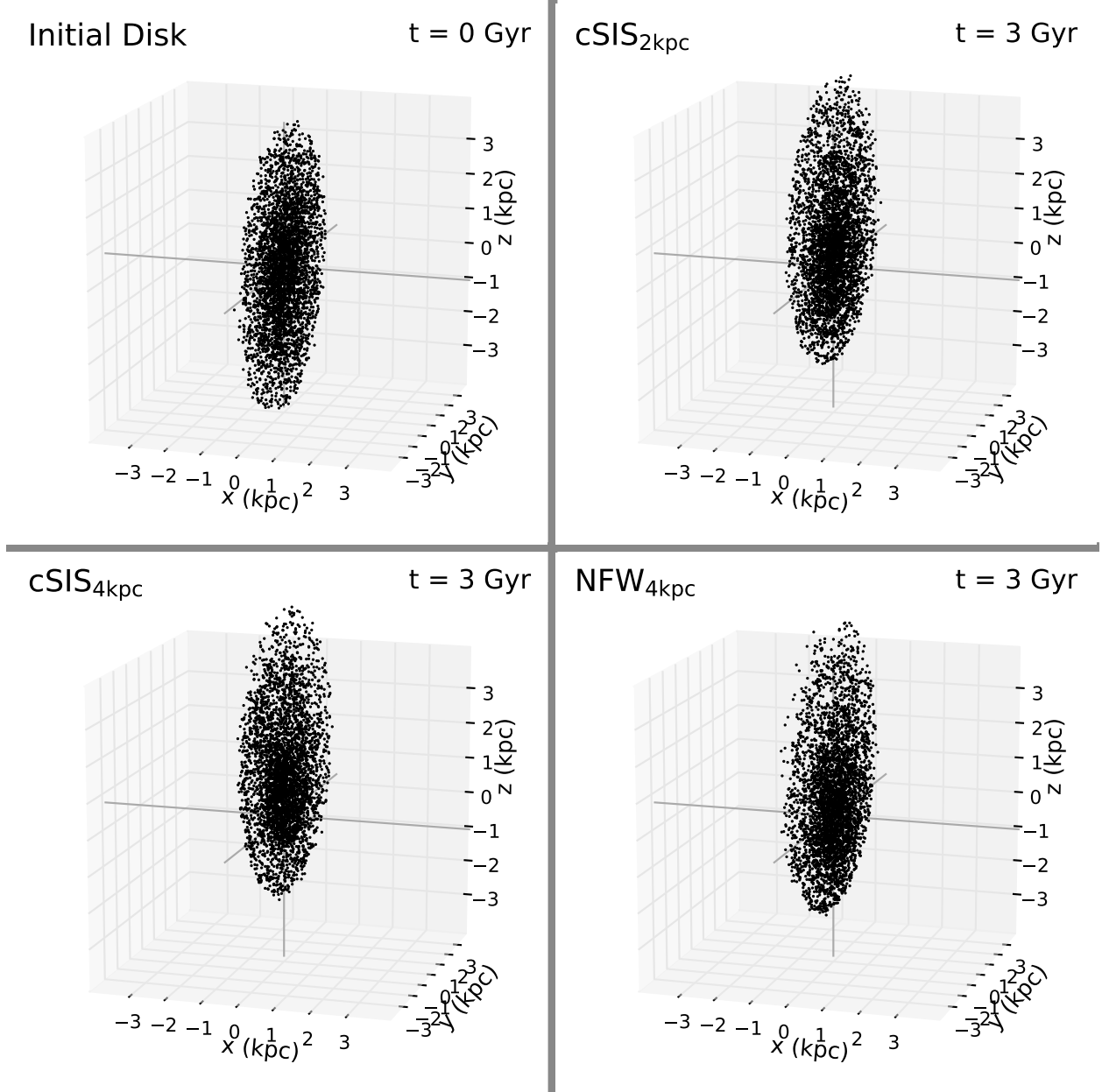


Fig. 7.— The change in the morphology of stellar disks in infalling dwarf galaxies is shown for an edge-on orientation with respect to the neighboring galaxy. For details refer to the caption of Figure 6.



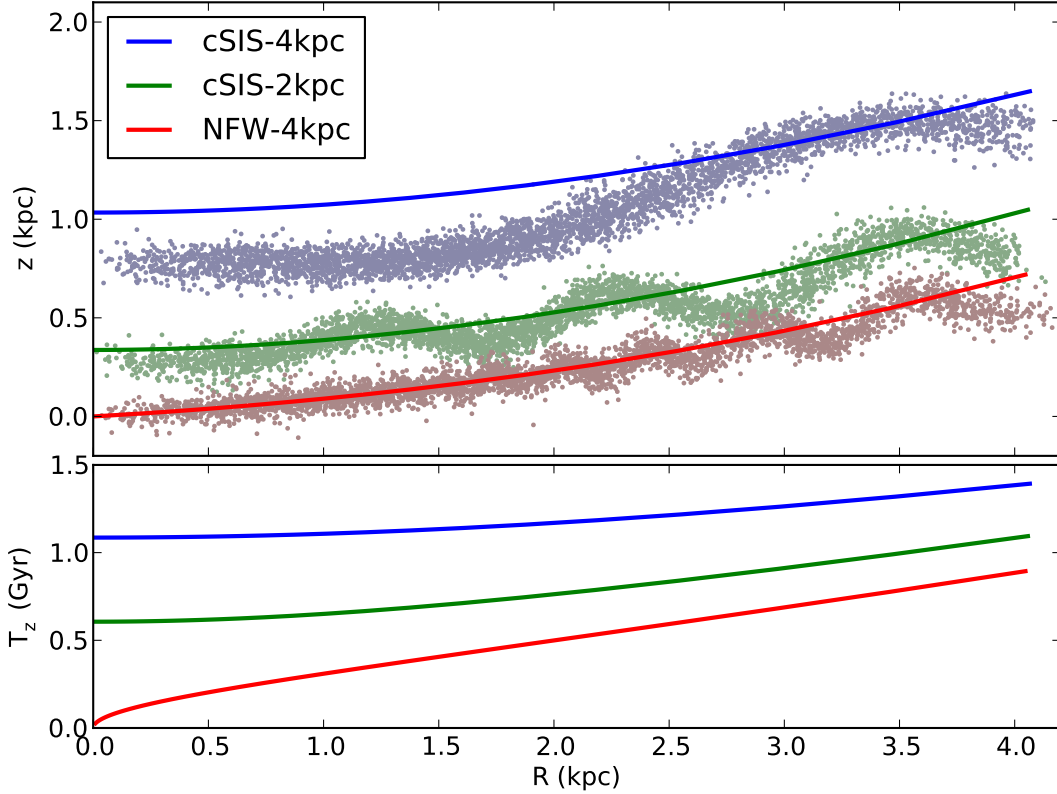


Fig. 8.— *Upper panel:* The distribution of the height of stars  $z$  at different radii  $R$  in the face-on case (Fig. 6). The lines denote the minimum of the effective potential for stars of increasing  $R$  (and angular momentum). The stars don't lie precisely at this minimum because their orbits are generally inclined, meaning they oscillate vertically about the minimum of the effective potential. *Lower panel:* the oscillation period  $T_z$  as a function of radius. Because the integration lasts 3Gyr, we'd expect the number of oscillations to be roughly equal to  $n = 3/(T_z/\text{Gyr})$ . For the NFW case,  $T_z$  increases rapidly with radius, which leads to the narrow oscillations in the disk.

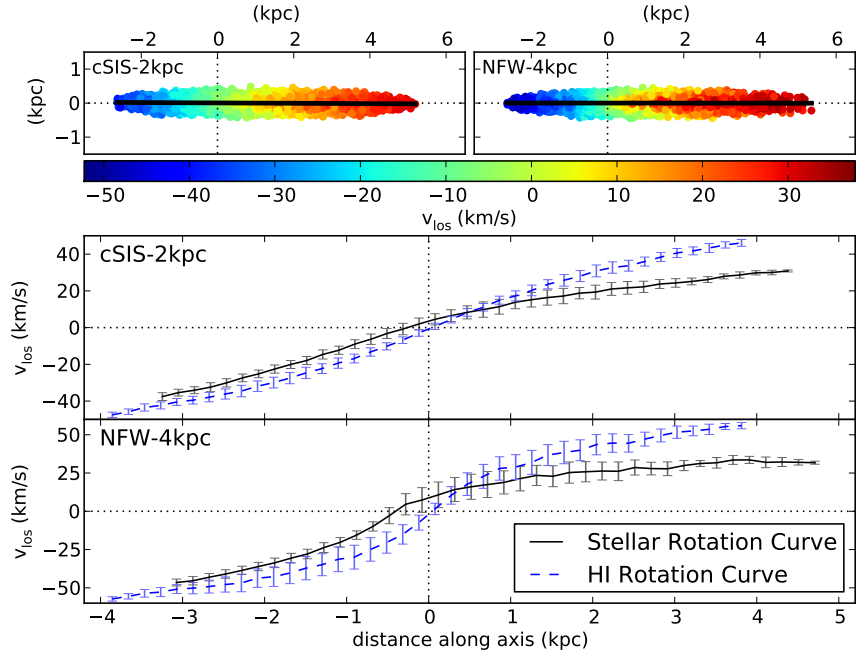


Fig. 9.— *Upper panels:* A near edge-on view of the final disk from the edge-on infall case (Fig. 7). We show only the  $\text{NFW}_{4\text{kpc}}$  halo and the  $\text{cSIS}_{2\text{kpc}}$  halo here; the rotation curve of  $\text{cSIS}_{4\text{kpc}}$  is qualitatively similar to that of  $\text{cSIS}_{2\text{kpc}}$ . Stars are color-coded by their radial velocity in km/s. Black lines denote the principal axis of the stellar distribution used to define the rotation curves. *Lower panels:* The HI and stellar rotation curves along the major axis of each galaxy. Two effects are apparent. First, because the HI disk is not dense enough to be self-shielded, it feels a stronger gravitational attraction to the dark matter and has a faster overall rotation. Second, the self-screened stellar disk lags the halo, leading to asymmetric distortions in the rotation curve of the disk. This effect is more pronounced for a steeper core.